Parameter scaling and practical design of TME lattice

Yi Jiao[1,2], Yunhai Cai[1], Alexander W. Chao[1]
1, SLAC National Accelerator Laboratory, Stanford University, California, 94025
2, Institute of High Energy Physics, CAS, Beijing, 100049

[Abstract] It is a challenge to produce a practical design of an electron storage ring with a theoretical minimum emittance (TME) lattice of ultra low emittance, e.g. down to a level of several pico-meters, due to the very strong focusing and the extremely large natural chromaticity associated with the lattice design. To help dealing with this challenge, it is customary to scale the parameters and look for a best solution guided by these scaling properties. In this paper, the parameter scaling is summarized, and it is argued that, with the lattice configuration with defocusing quadrupoles closer to the dipoles or simply with combined-function defocusing dipoles, one can reach a good balance of the low emittance and relatively small natural chromaticity, with phase advance per half cell below π/2. A 10 pm TME lattice for PEP-X is shown as demonstration of the design procedure.

Keywords: TME lattice, parameter scaling, ultra low emittance, electron storage ring

1. Introduction

Emittance is one of the most important parameters for electron storage rings. Ultra low emittance allows high luminosity in electron-positron colliders or high brightness in modern synchrotron light sources. During the past few decades, many efforts have been made to study the theoretical minimum emittance (TME) [1] and its concrete implementations (see, e.g. ref. [2]).

A TME cell usually consists of one normal or combined-function dipole with length L_B and bending angle θ and a few families of quadrupoles. The beta function β_{x0} and dispersion D_{x0} are minimal in the middle of the dipole (for simplicity, the subscript x of the Courant-Snyder parameters is ignored in the following context).

In Ref. [1], the TME condition for normal dipole is obtained as

$$\beta_0^* = \frac{L_B}{2\sqrt{15}}, \quad D_0^* = \frac{L_B^2}{24\rho}, \quad \varepsilon_{x0}^* = \frac{C_q \gamma_L^2 \theta^3}{12\sqrt{15} J_x}, \quad \mu_x^* = 142 \text{ degrees} \tag{1}$$

where C_q = 3.83*10^{-13}m; γ_L is the Lorenz factor; $\rho = L_B/\theta$ is the bending radius of dipole; J_x is the horizontal damping partition number, which is very close to 1 for normal dipole with small bending angle; μ_x is the phase advance per half cell. An asterisked quantity means the quantity is evaluated when the exact TME condition is fulfilled.

Normally, it is not difficult to realize the exact TME condition in a practical lattice design. However, in the case of designing a TME lattice with ultra low emittance, e.g.

down to a level of several pico-meters, it requires very strong focusing quadrupoles and in turn requires extremely strong sextupoles to correct the natural chromaticity. They lead to large geometric and chromatic nonlinear aberrations, causing the difficulty of dynamic aperture optimization. In order to maintain the natural chromaticity at a reasonable level, we prefer relatively weak focusing, phase advance smaller than μ_x^*, and reach emittance close to, rather than at the exact TME condition.

Therefore it is essential to understand the variation behaviors of important parameters in the neighborhood of the exact TME conditon, such as the phase advance per half cell μ_x, relative emittance ε_r, relative beta function β_r and dispersion D_r. In this paper, we call it "parameter scaling",

$$\varepsilon_r = \frac{\varepsilon_{x0}}{\varepsilon_{x0}^*}, \beta_r = \frac{\beta_0}{\beta_0^*}, D_r = \frac{D_0}{D_0^*} \tag{2}$$

The overall picture of the parameter scaling of a TME lattice discussed in a previous study [3] and maybe in intuition is that, as μ_x moves down from μ_x^*, the relative emittance ε_r will increase monotonically. Actually, it is not exactly correct. In Sec. 2, the parameter scaling of the TME cell with normal dipole is studied systematically. We find that a discontinuity emerges at $\mu_x = \pi/2$ along with ε_r rapid increasing as μ_x decreases towards $\pi/2$. After crossing the discontinuity at $\mu_x = \pi/2$, however, the ε_r exhibits a local minimum at μ_x around 80 degrees. The discontinuity is caused by the fact that the cases of μ_x above and below $\pi/2$ are physically related to two different lattice configurations, i.e. TME cell with horizontal focusing quadrupole (QF) or defocusing quadrupole (QD) closer to the dipole. The latter configuration (μ_x below $\pi/2$ and QD close to the dipole) can enable us to achieve relative low emittance as well as reasonable natural chromaticity.

We then expand the analysis to TME lattice with combined-function defocusing dipoles in Sec. 3. It is found that, the TME cell with defocusing dipole allows of lower emittance than that with normal dipole, especially in the case of μ_x below $\pi/2$. In sec. 4, we discuss the principles in practical ultra-low emittance lattice design based on the parameter scaling study and present a compact TME lattice for PEP-X storage ring with emittance of 10 pm as demonstration.

2. TME cell with normal dipole

2.1 Relative emittance and phase advance per half cell

The equilibrium emittance of TME cell with a normal dipole of small bending angle can be written as [1]

$$\begin{aligned}\varepsilon_{x0} &= \frac{C_q \gamma_L^2 \theta^3}{J_x} F = \frac{C_q \gamma_L^2 \theta^3}{J_x} < H >_{dip} \frac{\rho^2}{L_B^3} \\ &= \frac{C_q \gamma_L^2 \theta^3}{J_x} \cdot \left(\frac{3L^5 + 960 D_0^2 L \rho^2 + 80 L^3 (\beta_0^2 - D_0 \rho)}{960 L^4 \beta_0}\right)\end{aligned} \tag{3}$$

where $\langle H \rangle_{dip}$ is the average of Courant-Snyder dispersion invariant over the dipole. Substituting the scaled parameters (Eq. (2)) into the above equation, one obtain the expression of ε_r in terms of D_r and β_r [3],

$$\varepsilon_r = \frac{9 - 10D_r + 5D_r^2 + 4\beta_r^2}{8\beta_r} \tag{4}$$

In addition, the expression of μ_x in terms of β_r and D_r was obtained in Ref. [4],

$$\tan \mu_x = \frac{2\sqrt{3}}{\sqrt{5}} \frac{\beta_r}{D_r - 3} \tag{5}$$

Eqs. (4) and (5) show that both ε_r and μ_x are related to β_r and D_r. Yet, we can not view the variation behavior of ε_r with respect to μ_x unless we obtain the relationship between β_r and D_r. In Ref. [3], a correlation between β_r and D_r, $dD_r/d\beta_r = 0$, was used to obtain the parameter scaling equations, which, however, do not apply well in a compact TME lattice design with ultra-low emittance and especially with μ_x below $\pi/2$.

In the following, we will derive approximate expressions of β_r in terms of D_r for the cases with μ_x above and below $\pi/2$, which we will then use to reveal the typical parameter variation behavior in a TME lattice.

2.2 Relationship between β_r and D_r when $\mu_x > \pi/2$

Generally, a TME cell can be divided into (HD, Ptd, Ptd, HD), where HD is half of the dipole, and Ptd is the part outside the dipole including drifts and quadrupoles.

It is convenient to introduce the 3-by-3 transfer matrix of the horizontal motion which includes the propagation of off-momentum rays [5]. In the case of small bending angle, the transfer matrices can be written as

$$M_{hd} = \begin{pmatrix} 1 & L_B/2 & L_B^2/8\rho \\ 0 & 1 & L_B/2\rho \\ 0 & 0 & 1 \end{pmatrix} \tag{6}$$

$$M_{ptd} = \begin{pmatrix} m_{11} & m_{12} & 0 \\ m_{21} & m_{22} & 0 \\ 0 & 0 & 1 \end{pmatrix} \tag{7}$$

where m_{11}, m_{12}, m_{21} are arbitrary values, while m_{22} is determined by the condition $Det\ M_{ptd} = 1$ [6]. Multiplying the matrices in sequence, one can obtain the periodic transfer matrix $M_{pcd} = M_{hd}.M_{ptd}.M_{ptd}.M_{hd}$ and the corresponding periodic transfer matrix MCS_{pcd} of the Courant-Snyder parameters at the dipole center.

The Courant-Snyder parameters are periodic in a standard TME cell, thus we have,

$$\begin{pmatrix} D_0 \\ D_0' \\ 1 \end{pmatrix} = M_{pcd} \begin{pmatrix} D_0 \\ D_0' \\ 1 \end{pmatrix}, \quad \begin{pmatrix} \beta_0 \\ \alpha_0 \\ \gamma_0 \end{pmatrix} = MCS_{pcd} \begin{pmatrix} \beta_0 \\ \alpha_0 \\ \gamma_0 \end{pmatrix} \tag{8}$$

where the Courant-Snyder parameters at the dipole center are

$$\begin{pmatrix} D_0 \\ D_0' \\ 1 \end{pmatrix} = \begin{pmatrix} D_r \times \frac{L_B^2}{24\rho} \\ 0 \\ 1 \end{pmatrix}, \quad \begin{pmatrix} \beta_0 \\ \alpha_0 \\ \gamma_0 \end{pmatrix} = \begin{pmatrix} \beta_r \times \frac{L_B}{2\sqrt{15}} \\ 0 \\ \frac{2\sqrt{15}}{L_B \times \beta_r} \end{pmatrix}$$

For the exact TME condition, $D_r = 1$ and $\beta_r = 1$. Eq. (8) results in

$$m_{12} = -\frac{3}{5} L_B m_{11}, m_{21} = \frac{15}{4 L_B m_{11}}, m_{22} = -\frac{5}{4 m_{11}} \tag{9}$$

It shows that m_{12}, m_{21}, m_{22} all depends on m_{11}, which is a very strong constraint on the transfer matrix M_{ptd}.

In a practical design, one usually determine and fix the dipole parameters first and then match the optics by tuning the transfer matrix outside the dipole, i.e. M_{ptd}. Assuming the deviation of the transfer matrix from Eq. (9) is not large, we have

$$M_{ptd1} = \begin{pmatrix} m_{11} + d_{11} & -\frac{3}{5} L_B m_{11} + d_{12} & 0 \\ \frac{15}{4 L_B m_{11}} + d_{21} & -\frac{5}{4 m_{11}} + d_{22} & 0 \\ 0 & 0 & 1 \end{pmatrix} \tag{10}$$

where d_{11}, d_{12}, d_{21} are arbitrary small values and d_{22} is determined by $Det\ M_{ptd1} = 1$. With M_{ptd1} and M_{hd}, we can calculate the new periodic transfer matrices M_{pcd1} and MCS_{pcd1}.

Again, using the periodic condition (Eq. (8) with M_{pcd1}, MCS_{pcd1} and arbitrary D_r, β_r) to obtain the expressions of D_r and β_r in terms of d_{11}, d_{12}, d_{21} and m_{11},

$$D_r = -3 \times \frac{20 d_{12}(15 + 4 d_{21} m_{11}) + L_B[5 d_{11}(15 + 4 d_{21} L_B m_{11}) - m_{11}(25 + 28 d_{21} L_B m_{11})]}{5 L_B (d_{11} + m_{11})(15 + 4 d_{21} L_B m_{11})}$$

$$\beta_r = \sqrt{\frac{3}{5}} \frac{\sqrt{-(10 d_{12} + 5 d_{11} L_B - L_B m_{11})}}{L_B \sqrt{(d_{11} + m_{11})^2 (15 + 4 d_{21} L_B m_{11})}} \tag{11}$$
$$\times \sqrt{[10 d_{12}(15 + 4 d_{21} L_B m_{11}) + L_B(m_{11}(25 - 4 d_{21} L_B m_{11}) + 5 d_{11}(15 + 4 d_{21} L_B m_{11}))]^2}$$

With substitutions, $t = d_{21} * L_B * m_{11}$, $s = d_{11} / m_{11}$ and $r = d_{12} / (m_{11} * L_B)$, we simplify the

above equation as

$$D_r = -3 \times \frac{(-25 - 28t + 20r(15+4t) + 5s(15+4t))}{5(1+s)(15+4t)}$$
$$\beta_r = \sqrt{\frac{3}{5}} \frac{\sqrt{(1-10r-5s)(25-4t+10r(15+4t)+5s(15+4t))}}{\sqrt{(1+s)^2(15+4t)}} \quad (12)$$

Note that there are three independent variables r, s and t in the above expressions. In order to obtain a simple relationship between D_r and β_r, we note that comparing with the other two variables, s is much more closely related to the shift of the phase advance. Thus only keep s and let t, $r \to 0$, Eq. (12) becomes

$$D_r \approx \frac{25-75s}{25(1+s)}$$
$$\beta_r \approx \sqrt{\frac{(1-5s)(25+75s)}{25(1+s)^2}} \quad (13)$$

Then we obtain the approximate expression of β_r in terms of only D_r,

$$\beta_r \approx \frac{1}{2}\sqrt{-3(3-D_r)^2 + 8(3-D_r)} \quad (14)$$

Eq. (14) applies for the cases with parameter deviations not large from the exact TME condition.

It is worth noting that, keep t or r and let other two variables tend to zero, one can obtain similar expressions of β_r in terms of only D_r.

In order to clarify the variation behavior of β_r with respect to D_r predicted by Eq. (14), we design a lattice at the exact TME condition (Fig.1), vary the normalized gradients of quadrupoles randomly in a range of 0.4 m^{-2} and the drift lengths in a range of 0.2 m around the original values, and then plot the stable solutions in Fig. 2. It shows that the agreement between the analytical predictions and the numerical calculations is pretty well.

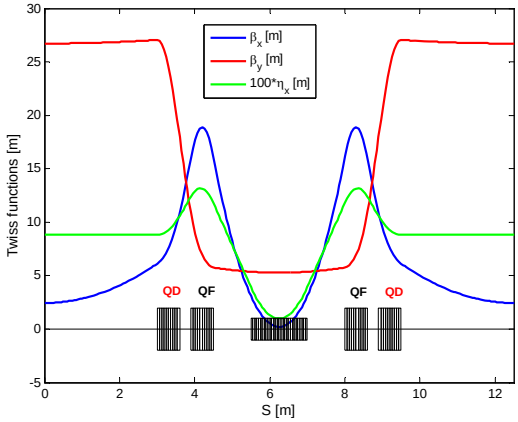

Fig. 1 One cell of the TME lattice with QF closer to the dipole. The cell length is 12.5m, L_B = 1.5m, $\theta = \pi/20$ and $\varepsilon_r = 1$.

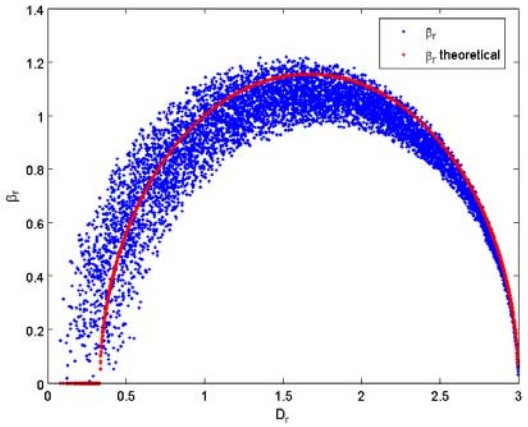

Fig. 2 Variations of β_r obtained numerically and analytically with respect to D_r.

2.3 Relationship between β_r and D_r when $\mu_x < \pi/2$

When μ_x is below $\pi/2$, Eq. (14) will not work any longer because the transfer matrix M_{ptd} already deviates from Eq. (9). Therefore we first discuss the constraints on the transfer matrix M_{ptd} at $\mu_x = \pi/2$, and then explore the relationship between β_r and D_r by applying small perturbations to the transfer matrix.

Eq. (5) shows that $D_r = 3$ when $\mu_x = \pi/2$. Using the periodic condition (Eq. (8) with $D_r = 3$) and the symplectic condition, we obtain

$$m_{21} = -\frac{2}{L_B m_{11} + 2m_{12}}, m_{22} = \frac{L_B}{L_B m_{11} + 2m_{12}} \tag{15}$$

In addition, the values of m_{11} and β_r are related to each other. If $m_{11} = 0$, β_r and m_{12} are arbitrary; if $m_{11} \neq 0$, β_r tends to 0 (as beta function can never vanish, this condition requires a beta function at the dipole center as small as possible) and $m_{12}/m_{11} = -L_B/2$.

It should be mentioned here that, the first case with $m_{11} = 0$ is very hard to realize in a practical TME lattice design, in which, we are interested in not only low emittance but also small cell length as much as possible, namely, compact lattice layout. In such a compact TME cell, the drift lengths are usually set to available minimal values, with very limited adjustable range. Two or even one family of quadrupoles are used to match the optics. The primary goal of the optics matching is to squeeze the horizontal Courant-Snyder parameters at the dipole center, control the maximal beta functions (typically < 35m), and tune the phase advance to appropriate value to cancel the nonlinear geometric aberrations. There are usually not enough variables to realize the condition $m_{11} = 0$ while satisfying the goals listed above. On the other hand, no constraints are imposed on the element m_{11} in the second case, and the condition $\beta_r \to 0$ as $D_r = 3$ is consistent with Eq. (14) (see also Fig. 2). Thus in what follows, we confine the derivation to the second case, i.e. $m_{11} \neq 0$, $\beta_r \to 0$ and $m_{12}/m_{11} = -L_B/2$.

Now we consider the case of μ_x slightly below $\pi/2$. In this case, the matrix M_{ptd} can be written as

$$M_{ptd} = \begin{pmatrix} m'_{11} & m'_{12} & 0 \\ m'_{21} & m'_{22} & 0 \\ 0 & 0 & 1 \end{pmatrix} \tag{16}$$

where the matrix components will tend to second case of above solutions when μ_x approaches $\pi/2$.

Calculate the 2-by-2 transfer matrix of the half cell $M_{hc}=M_{ptd}.M_{hd}$ and write it in terms of Courant-Snyder parameters,

$$\begin{pmatrix} m'_{11} & \frac{L_B}{2}m'_{11}+m'_{12} \\ m'_{21} & \frac{L_B}{2}m'_{21}+m'_{22} \end{pmatrix} = \begin{pmatrix} \sqrt{\frac{\beta_{cb}}{\beta_0}}\cos\mu_x & \sqrt{\beta_{cb}\beta_0}\sin\mu_x \\ -\sin\mu_x/\sqrt{\beta_0\beta_{cb}} & \sqrt{\frac{\beta_0}{\beta_{cb}}}\cos\mu_x \end{pmatrix} \tag{17}$$

where "*cb*" indicate the cell boundary. The conditions of $\alpha_x = 0$ at the dipole center and the cell boundary are used to obtain the matrix on the R.H.S. of Eq. (17).

From the one-to-one correspondence of the matrix components in Eq. (17), we have

$$\beta_0 \tan\mu_x = \frac{L_B}{2} + a \tag{18}$$

with $a = m'_{12}/m'_{11}$.

Due to β_0 is always positive, for $\mu_x < \pi/2$, the L.H.S. of Eq. (18) is positive. Then the infimum of a is $-L_B/2$.

Use Eqs. (1), (2), (5) and (18) to cancel μ_x,

$$\frac{\beta_r^2}{D_r - 3} = \frac{5}{2} + \frac{5a}{L_B} \tag{19}$$

Then substitute above equation to Eq. (3) to cancel D_r, we obtain

$$\varepsilon_r = \frac{1}{2}\left(\beta_r + \frac{1}{\beta_r}\right) + \frac{\beta_r}{10}\left(\frac{L_B\beta_r}{2a+L_B} + \frac{5}{\beta_r}\right)^2 \tag{20}$$

It is clear that, no matter what the value of a is, the relative emittance ε_r will be large if β_r is much smaller or larger than 1. If a is smaller than zero, or even close to $-L_B/2$, ε_r will also be large. Only moderate β_r and positive a allow relative small ε_r.

The expression of β_{cb} can be obtained by multiplying the MCS_{hc} derived from M_{hc} with the vector of Courant-Synder parameters at the dipole center,

$$\beta_{cb} = m_{11}'^2 [\frac{\beta_r L_B}{2\sqrt{15}} + \frac{2\sqrt{15}}{\beta_r L_B}(a + \frac{L_B}{2})^2] \tag{21}$$

For nonzero m_{11}', β_{cb} will increase with a. To avoid large β_{cb}, moderate a is required.

Consider a varying from 1 to 50 m and L_B = 2m, we calculate the ε_r with different β_r, as shown in Table 1 and Fig. 3. The deviation of ε_r is small with a changing dramatically, especially for small β_r. It is therefore possible to find a quasi-relationship between ε_r and β_r.

Table 1. ε_r versus β_r, `with` a varying from 1 to 50 m and L_B = 2m

β_r	ε_r (max)	ε_r (min)	ε_r (mean)	$\Delta\varepsilon_r$
0.5	6.50	6.27	6.38	0.12
1	4.02	3.53	3.77	0.25
2	4.68	2.56	3.61	1.05
3	6.35	2.83	4.59	1.75
4	6.35	2.83	4.59	1.76
5	8.73	3.20	5.96	2.76

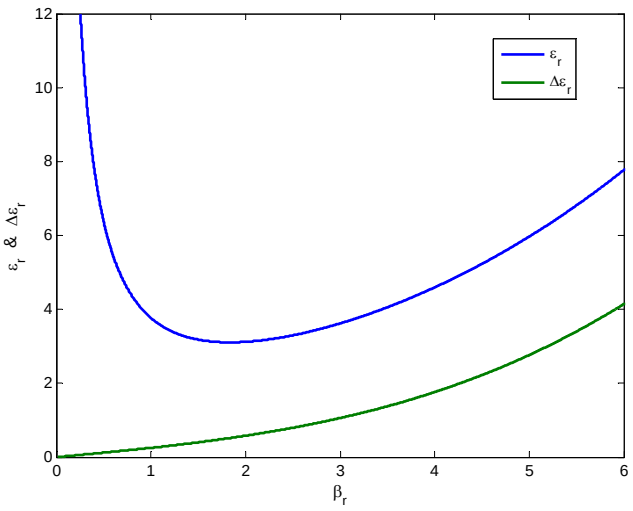

Fig.3 Average ε_r and $\Delta\varepsilon_r$ with β_r, while a varying from 1 to 50 m and L_B = 2m.

Numerical simulations are undertaken to verify the analysis. With the TME lattice shown in Fig.4, we randomly vary the normalized quadrupole gradients in a range of 4 m^{-2} around the original values and drift lengths in a range of 1m (but keep the total cell length smaller than 7.5 m), and then record all the stable solutions with ε_r smaller than 10 and plot the corresponding β_r^2 versus (D_r – 3) in Fig. 5. Instead of uniformly distributed, most of the points locate around a straight line. The slope A is obtained by fitting the data.

We simulate the cases with dipole length from 0.8 to 5m, and summarize the results in

Fig. 6. We find that, Eq. (19) with a = 1.5 m can well describe the variation of β_r^2 with (D_r − 3), for a compact TME lattice with QD closer to the dipole, low ε_r and phase advance per half cell below π/2.

With straightforward calculation, we obtain the expression of ε_r in terms of μ_x,

$$\varepsilon_r \cong \frac{\sqrt{15}}{\tan\mu_x} + \frac{\sqrt{3}\tan\mu_x}{\sqrt{5}B} + \frac{\sqrt{15}}{2}\left(\frac{1}{\tan\mu_x} + \frac{3}{\tan^3\mu_x}\right)B \qquad (22)$$

with $B = 1 + 3\,L_B$.

The β_r and D_r as function of μ_x can also be derived. They are omitted here due to lengthy expressions.

Once the dipole length is determined, one can view the variation behaviors of the parameters, i.e. ε_r, μ_x, D_r and β_r, regardless of the concrete setting of quardupole strengths and drift lengths outside the dipole.

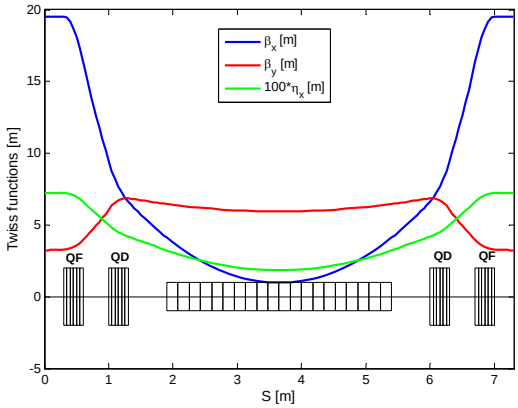

Fig. 4 One cell of the TME lattice with QD closer to the dipole. The cell length is 7.3m, L_B = 3.5m, θ = π/99, D_r =4, β_r =2.16, ε_r = 3.9 and μ_x=73.4 degrees.

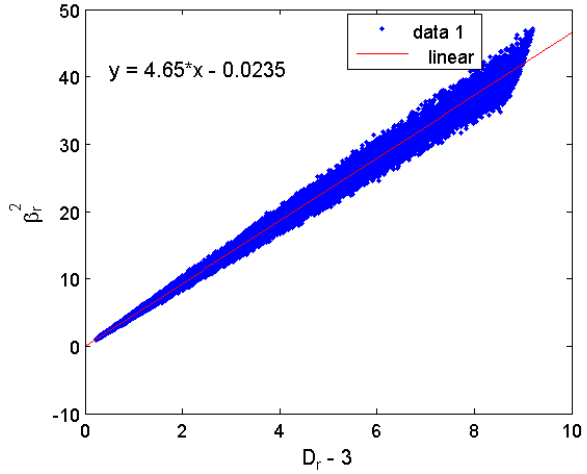

Fig. 5 Plot of β_r^2 with respect to (D_r −3), L_B = 3.5m.

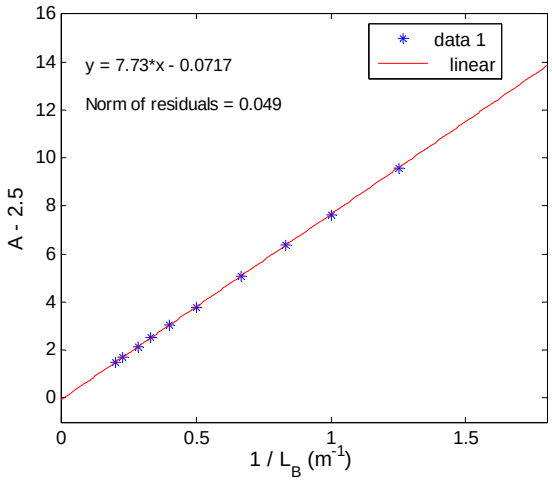

Fig. 6 Plot of (A-2.5) with respect to $1/L_B$.

2.4 Discussion

We summarize the scaling of the parameters of ε_r, μ_x, D_r and β_r for TME cell with normal dipole using Eqs. (4), (5), (14) and (19) with a = 1.5 m in Fig. 7 with L_B = 3.5m. It shows that, the ε_r decreases as μ_x moves down from the μ_x^* until $\mu_x = \pi/2$, where a discontinuity occurs along with rapidly increasing ε_r. For μ_x below $\pi/2$, the ε_r reaches a local minimum (~3) at μ_x around 80 degrees.

The parameter variation behaviors are different in the cases of μ_x above and below $\pi/2$. It is caused by the fact that the two cases are physically related to two different lattice configurations, i.e. TME cell with QF or QD closer to the dipole (see Fig. 1 and 3). For the latter configuration, the horizontal focusing is relatively weak, the beta and dispersion functions are not much squeezed, and the phase advance per half cell μ_x is usually below $\pi/2$. As a rule of thumb, the smaller the phase advance is, the smaller the natural chromaticity will be. Now, we arrive at a TME lattice with more relaxed optics than that corresponding to the exact TME condition, relatively low emittance ($\varepsilon_r \sim 3$) and reasonable natural chromaticity.

The scaling curves in Ref. [3] are also plotted for comparison. We can see that, it does not predict the discontinuity in the parameter scaling curves at $\mu_x = \pi/2$ and it does not reveal the difference between the two lattice configurations.

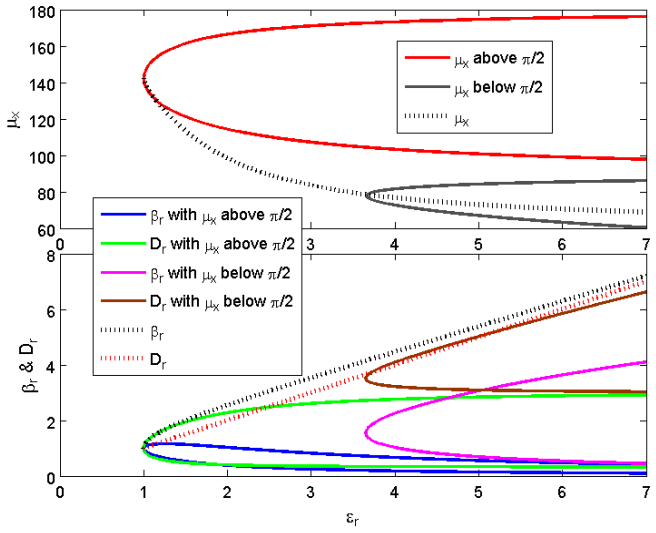

Fig. 7 Variations of μ_x (upper) and D_r, β_r (lower) with respect to ε_r for TME cell with normal dipole. The dashed lines indicate the parameter scaling curves obtained with $dD_r/d\beta_r = 0$ in Ref. [3].

3. TME cell with combined-function defocusing dipole

In this section, we will firstly show that, the TME cell with combined-function defocusing dipole (DD) can enable us to achieve lower minimal emttiance than that with normal dipole (ND). And then, we will present the parameter scaling in TME cell with combined-function defocusing dipole, and compare it with that in TME cell with normal dipole.

3.1 Minimal emittance with combined-function defocusing dipole

The transfer matrix of a combined-function defocusing dipole can be written as

$$M_{dfd} = \begin{pmatrix} \cosh(\sqrt{K}L_B) & \dfrac{\sinh(\sqrt{K}L_B)}{\sqrt{K}} & \dfrac{-1+\cosh(\sqrt{K}L_B)}{K\rho} \\ \sqrt{K}\sinh(\sqrt{K}L_B) & \cosh(\sqrt{K}L_B) & \dfrac{\sinh(\sqrt{K}L_B)}{\sqrt{K}\rho} \\ 0 & 0 & 1 \end{pmatrix} \tag{23}$$

The equilibrium emittance for a TME cell with combined-function defocusing dipole is

$$\varepsilon_{x0}(DD) = \frac{C_q \gamma_L^2 \theta^3}{J_x(DD)} F(DD) \tag{24}$$

$$F(DD) = \frac{8(1+D_0 K\rho) - \sqrt{K}L_B[3+K(-\beta_0^2 + 2D_0\rho(2+D_0 K\rho))]}{2K^{5/2}L_B^5\beta_0} \tag{25}$$

$$J_x(DD) = 1 - \frac{\oint (D(s)/\rho^3 - 2KD(s)/\rho)ds}{\oint 1/\rho^2 ds} = 1 - \frac{\int_{L_B} (D(s)/\rho - 2KD(s)\rho)ds}{L_B} \tag{26}$$

with $D_x(s) = (-1 + \cosh(\sqrt{K}s))/K/\rho + D_0 \cosh(\sqrt{K}s)$

There are two factors to be considered, i.e. $F(DD)$ and $J_x(DD)$. The minimal value of $F(DD)$ is reached at the condition

$$\beta_0^*(DD) = \frac{\sqrt{4 + KL_B^2 - 4\cosh(\sqrt{K}L_B) + \sqrt{K}L_B \sinh(\sqrt{K}L_B)}}{\sqrt{-K^2L_B^2 + K^{3/2}L_B \sinh(\sqrt{K}L_B)}} \tag{27}$$

$$D_0^*(DD) = \frac{-\sqrt{K}L_B + 2\sinh(\sqrt{K}L_B/2)}{K^{3/2}L_B\rho} \tag{28}$$

The corresponding minimal emittance is

$$\varepsilon_{x0}^*(DD) = C_q\gamma_L^2\theta^3 \times$$
$$\frac{\rho^2\sqrt{(4 + KL_B^2 - 4\cosh(\sqrt{K}L_B) + \sqrt{K}L_B \sinh(\sqrt{K}L_B))}\sqrt{K^{3/2}L_B \sinh(\sqrt{K}L_B) - K^2L_B^2}}{KL_B^3(-2 - KL_B^2 + 4K\rho^2 + (2 - 4K\rho^2)\cosh(\sqrt{K}L_B))} \tag{29}$$

On the limit $K \to 0$, Eqs. (27) - (29) are reduced to Eq. (1).

Although the $F_{min}(DD)$ is larger than $F_{min}(ND)$, as shown in Fig. 8, the damping partition number $J_x(DD)$ also increases with the increasing $K^{1/2}L_B$ and can be larger than 1. To clarify the total effect of the combined-function defocusing dipole, we scale the $\varepsilon_{\min}$(DD) with $\varepsilon_{\min}$(ND),

$$\frac{\varepsilon_{\min}(DD)}{\varepsilon_{\min}(ND)} = \frac{\sqrt{15}(12 - \theta^2)\sqrt{[t^2 - t\sinh(t)]\cdot[-4 - t^2 + 4\cosh(t) - t\sinh(t)]}}{t[t^4 - 2\theta^2 - t^2(-4 + \theta^2) + (-4t^2 + 2\theta^2)\cosh(t)]} \tag{30}$$

where $t = K^{1/2}L_B$ and θ is the bending angle.

Fig. 9 shows the contour map of the $\varepsilon_{\min}$(DD)/$\varepsilon_{\min}$(ND) with respect to t and θ. We can see that, the scaling factor is nearly always smaller than 1, varying slowly with θ but quickly with t. In the case of t =1 and θ = π/99, $\varepsilon_{\min}$(DD)/$\varepsilon_{\min}$(ND) = 0.89.

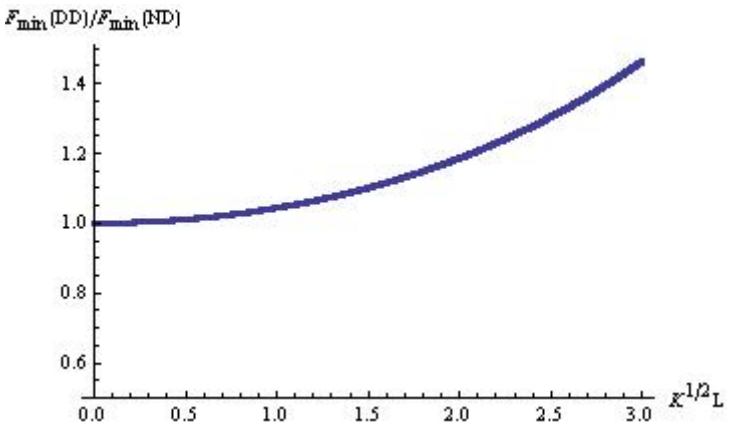

Fig. 8 $F_{min}(DD)/F_{min}(ND)$ variations with respect to $t = K^{1/2}L$.

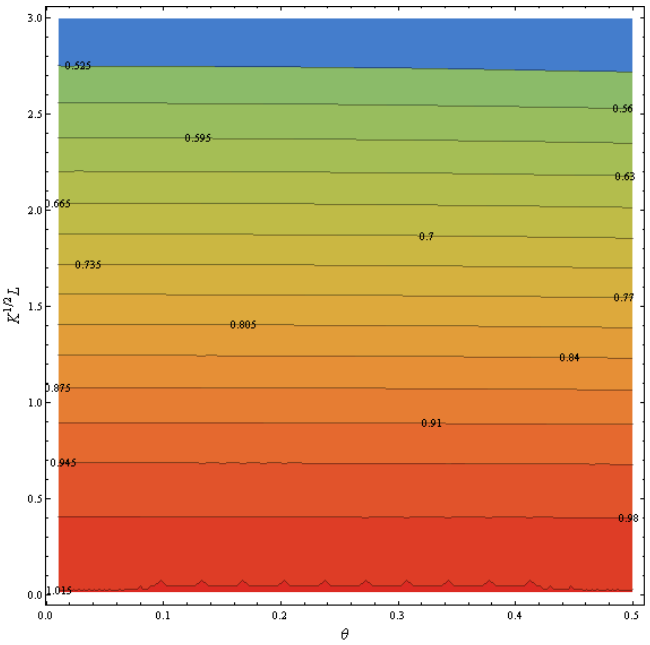

Fig.9 Contour map of $\varepsilon_{\min}(DD)/\varepsilon_{\min}(ND)$ with respect to $t = K^{1/2}L_B$ and θ.

3.2 Relative emittance and phase advance per half cell

Again, we define three non-unit scaled parameters,

$$\varepsilon_r(DD) = \frac{\varepsilon_{x0}(DD)}{\varepsilon^*_{x0}(DD)}, D_r(DD) = \frac{D_0(DD)}{D^*_0(DD)}, \beta_r(DD) = \frac{\beta_0(DD)}{\beta^*_0(DD)} \tag{31}$$

At a slight risk of confusion, we simply denote as ε_r, D_r, and β_r in what follows in Sec. 3.

We obtain the expression of ε_r in terms of D_r and β_r by inserting the scaled parameters into Eq. (31),

$$\varepsilon_r = \frac{-(t^4 - 2\theta^2 - t^2(-4+\theta^2) + (-4t^2 + 2\theta^2)\cosh(t))}{2\beta_r(4 + t^2 - 4\cosh(t) + t\sinh(t))} \times$$
$$\frac{4\beta_r^2 + 8D_r - 4D_r^2 + 3t^2 + \beta_r^2 t^2 - 4D_r^2 t^2 + 2D_r^2 t^2 - 4(\beta_r^2 + 2D_r - D_r^2)\cosh(t) - 8(D_r - 1)^2 t\sinh(t/2) + t\sinh(t) + \beta_r^2 t\sinh(t)}{(4D_r t^2 + t^4 - 2D_r\theta^2 - t^2\theta^2 + 2D_r(-2t^2 + \theta^2)\cosh(t) - 2(D_r - 1)t(-2t^2 + \theta^2)\sinh(t/2)} \tag{32}$$

The phase advance per half cell is obtained as

$$\tan\mu_x = -\frac{\beta_r \sinh(\frac{t}{2})}{[\sqrt{K}L_B(D_r - 1 + \cosh(\frac{t}{2})) - 2D_r\sinh(\frac{t}{2})]} \times \sqrt{\frac{t(4 + t^2 - 4\cosh(t) + t\sinh(t))}{(\sinh(t) - t)}} \tag{33}$$

When $\mu_x = \pi/2$, the D_r will be

$$D_r(\mu_x = \pi/2) = \frac{t(1-\cosh(t/2)}{t-2\sinh(t/2)} \tag{34}$$

3.3 Relationship between β_r and D_r

We also derive the approximate analytical expression of β_r with D_r. Since the derivation is similar as in Sec. 2, the detailed procedure is omitted here.

In the case of μ_x above $\pi/2$, we have

$$\beta_r \approx \sqrt{\frac{(2(D_r-1)x+2x\cosh(2x)-D_r\sinh(2x))(-4x+\sinh(4x))}{-6Cx-4B(D_r-1)x\cosh(2x)+8Cx\cosh(4x)-2Cx\cosh(8x)+BD_r\sinh(4x)}}\times$$
$$\sqrt{\frac{(-2B+4C+2BD_r-4CD_r-2C\cosh(2x)+4C(D_r-1)\cosh(4x)+2C\cosh(6x))x+(3C-B)D_r\sinh(2x)-CD_r\sinh(6x)}{1+4x^2-\cosh(4x)+x\sinh(4x)}} \tag{35}$$

where

$$A = 5+32x^2-8\cosh(4x)+3\cosh(8x)-8x\sinh(4x)-4x\sinh(8x),$$
$$B = -64x^3+8x\cosh(4x)-8x\cosh(8x)+(32x^2-2)\sinh(4x)+(8x^2+1)\sinh(8x),$$
$$C = 8x+4x\cosh(4x)-3\sinh(4x),$$
$$x = t/4$$

And in the case of μ_x below $\pi/2$, we have

$$\beta_r^2 = (D_r - \frac{t(1-\cosh(t/2)}{t-2\sinh(t/2)})\times\frac{(-t/2+\sinh(t/2))(-t+\sinh(t))}{\sinh(t/2)(4+t^2-4\cosh(t)+t\sinh(t))}\times$$
$$\frac{2Bt\cosh(t/2)+2L_B\sinh(t/2)}{L_B\cosh(t/2)+Bt\sinh(t/2)} \tag{36}$$

where the coefficient B is about 1.5 m.

On the limit $t\to 0$ and $\theta\to 0$ if necessary, Eqs. (32), (33), (35), (36) are reduced to Eqs. (4), (5), (14) and (19).

3.4 Discussion

We summarize the scaling of the parameters of ε_r, μ_x, D_r and β_r for TME cell with combined-function defocusing dipole using Eqs. (32), (33), (35) and (36) in Fig. 10, with L_B = 3.5m and t = 1. The parameter scaling curves for the TME cell with normal dipole are also plotted for comparison. We can see that, with combined-function defocusing dipole, one can reach even lower ε_r in the case of μ_x below $\pi/2$. In addition, it is possible to use only one family of quadrupoles in a TME cell by adopting combined-function defocusing dipoles, which leads to a compact lattice layout, as will be shown in Sec. 4.

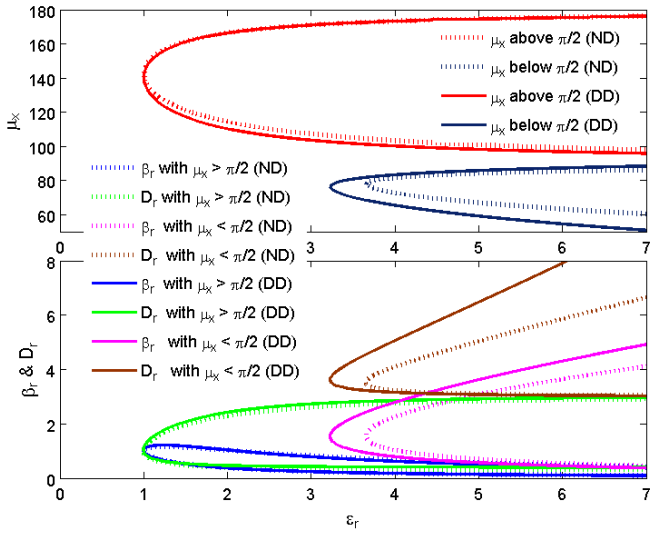

Fig .10 Variations of μ_x (upper) and D_r, β_r (lower) with respect to ε_r for TME cell with defocusing dipole. The dashed lines represent that of TME cell with normal dipole.

4. Practical design

4.1 Design consideration

As is shown above, to achieve low emittance, one should match the phase advance per half cell to be around 142 (exact TME condition) or 80 degrees (local minimal ε_r). On the other hand, to control the natural chromaticity, small phase advance, e.g. μ_x below $\pi/2$, is preferred, and it is best to set the phase advance to be $n\pi/N$ (n=1,2,3,…, N is the number of cells in one super-period) to cancel the geometric aberrations induced by the chromaticity correction sextupoles. Besides, one should reduce the length of TME cell as much as possible. As we know, the emittance is proportional to θ^3. For fixed circumference of a storage ring, smaller cell length means more TME cells, more dipoles, smaller bending angle of each dipole and thus smaller emittance.

4.2 Parameter selection

The 4.5 GeV ultra-low emittance synchrotron light source named as “PEP-X” was proposed recently [7]. The storage ring is planned to be built in the 2.2 km long PEP-II tunnel, which has 1.5 km arc length. At least thirty straight sections of 5m are required for synchrotron radiation experiments. Thus the 1.5 km arc is divided to 30 periods, and each period is 50 m. With rough estimation, the theoretical minimal emittance will be about 3 pm if the bending angle of each dipole $\theta = \pi/180$. So we totally use 390 combined-function defocusing dipoles (including 60 half angle dipoles) and adopt 11 standard TME cells and two matching cells in each period. The average length of each cell is 3.5 m, which calls for a compact lattice design.

4.3 Compact TME cell design

The sketch map of a standard TME cell is shown in Fig. 11. To save space, only one family of QF and a combined-function defocusing dipole are used to provide the transverse focusing. The length of quadrupole can be reduced to 0.15 m by using small aperture magnet [8]. The drift D1 is set to 0.25 m for focusing sextupoles (SF). The length of the drift between QF and dipole is 0.6 m, which is almost the minimal value for defocusing sextupoles (SD) and other devices. The defocusing dipole is 1.1 m long. The total length of the standard TME cell is 3.1 m.

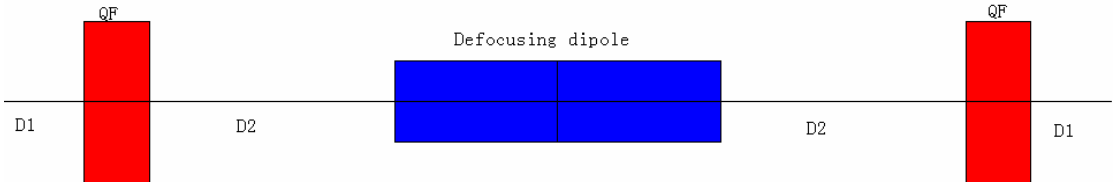

Fig. 11 Layout of the compact TME cell design

With the above parameter setting, we search for appropriate solution with the necktie diagram and contour plot of emittance and phase advance in the (K_f, K_d) space, as shown in Fig. 12. It shows that, the emittance of 10 pm can be approximately achieved at (μ_x, μ_y) = (5/11, 1/11) π. From the partial enlarged figure, we can see that the emittance does not reach a minimal value at $\mu_x = \pi/2$ but around 5π/11. The final lattice has emittance of 9.9 pm with ε_r(DD) = 3.3 and natural chromaticity of (−1.5, −0.4) per cell. The Courant-Snyder paramerters in one period of the storage ring are shown in Fig. 13.

5 Conclusions

The parameter scaling in TME cell with normal and defocusing dipole are presented. The relationship between the relative emittance ε_r and phase advance per half cell μ_x in terms of relative beta function β_r and relative dispersion D_r at the center of the dipole magnet are already known. To understand the scaling behaviors of the parameters, we should know the relationship between β_r and D_r. Strictly speaking, there is not one-to-one correspondence between these two parameters. However, basing on the assumption of small perturbations on the transfer matrices, approximate expressions of β_r in terms of only D_r for the cases of μ_x above and below π/2 are derived, which apply well when the lattice parameter deviations not large from the exact TME condition and the case with $\mu_x = \pi/2$, respectively.

The formulas enable us to view the parameter variations globally without carrying out numerous calculations. We find that emittance increase rapidly at $\mu_x = \pi/2$ and a local minimal emittance locates at μ_x about 80 degrees.

Throughout the paper, we highlight the TME cell with μ_x below π/2, which is physically related to the configuration with horizontal defocusing quadrupole closer to the dipole or simply with combined-function defocusing dipole. Due to the relative small phase advance and relaxed Courant-Snyder parameters, one can reach a good

balance of low emittance ($\varepsilon_r \sim 3$) and reasonable natural chromaticity. A 10 pm TME lattice for PEP-X is shown as demonstration.

Acknowledge

One of us (Yi Jiao) would like to thank Yuri Nosochkov in SLAC, USA and Gang Xu in IHEP, China for insightful discussions and help. This Work is supported by the Department of Energy under Contract No. DE-AC02-76SF00515.

Reference

[1] L.C. Teng, Fermilab Report No. TM-1269, 1984. Chun-xi Wang, Phys. Rev. ST Accel. Beams **12** 061001 (2009).

[2] S.Y. Lee, Phys. Rev. E 54 (1996), p. 1940. D. Einfeld, J. Schaper and M. Plesko, JOURNAL DE PHYSIQUE IV 4 (1994). K. Tsumaki, N. Kumagai, Nucl. Instr. and Meth. A 565 (2006) 394-405.

[3] J.P. Potier and L. Rivkin, CERN Report No. CERN-PS-97-020, 1997; P. Emma and T.O. Raubenhemier, Phys. Rev. ST Accel. Beams **4** 021001 (2001).

[4] L. Rivkin, in *Proceeding of the 7th International Worshop on Linear Colliders* (LC97), Zvenigorod, Russia, 1997, p. 509.

[5] A.W. Chao and M. Tigner, "Handbook of Accelerator Physics and Enginering", 3rd printing, World Scienfific, 2006, p. 65-66.

[6] E.D. Courant and H.S. Snyder, Ann. Phys. (Paris) **3**, 1 (1958).

[7] Yunhai Cai, et al, SLAC-PUB-13999 (2010).

[8] S.C. Leemann, et al, Phys. Rev. ST Accel. Beams **12** 120701 (2009).

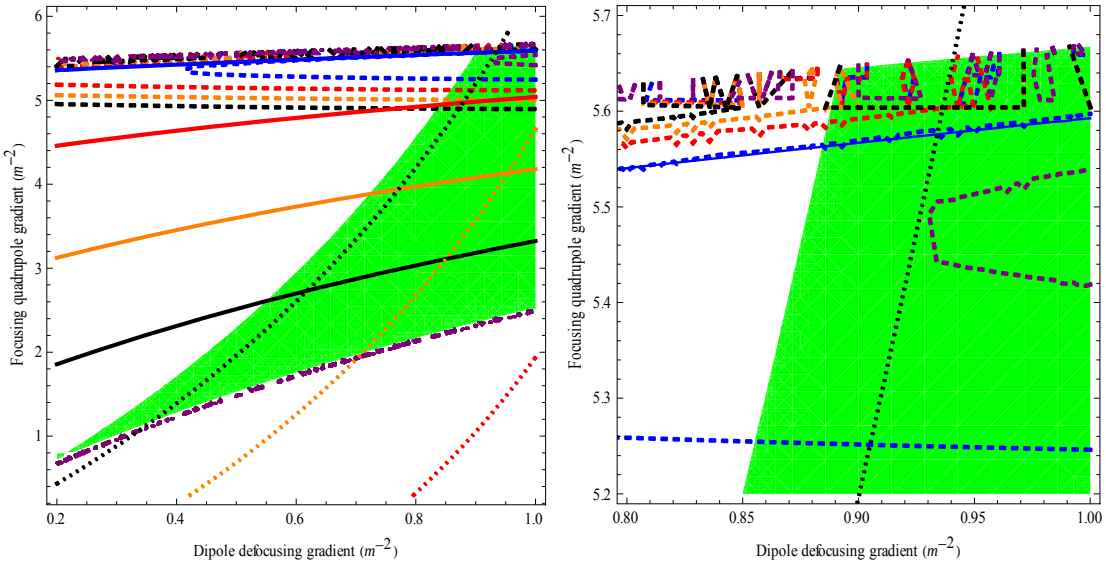

Fig. 12 Necktie diagram and contour plot of emittance and phase advance with gradients of the defocusing dipole and QF. Green area represents stable region. Left figure: solid lines, from lower to upper, represent μ_x = (2/11, 3/11, 4/11, 5/11) π; dotted lines, from left to right, represent μ_y = (1/11, 2/11, 3/11) π; dashed lines, from

lower to upper, ε_x = (13, 12, 11, 10, 9) pm. Right partial enlarged figure: solid blue line represents μ_x = 5/11π; dotted black line represents μ_y = 1/11π; blue dashed line represents ε = 10pm and purple dashed line for ε = 9pm.

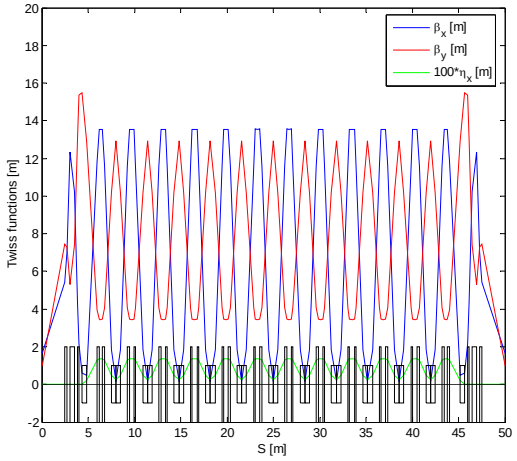

Fig. 13 Courant-Snyder parameters along one period of TME lattice for PEP-X storage ring